PERGAMON

International Journal of Heat and Mass Transfer 46 (2003) 251–262

International Journal of HEAT and MASS TRANSFER

www.elsevier.com/locate/ijhmt

Streamline upwind numerical simulation of two-dimensional confined impinging slot jets

T.H. Park [a], H.G. Choi [a], J.Y. Yoo [a,*], S.J. Kim [b]

[a] *School of Mechanical and Aerospace Engineering, Seoul National University, Seoul 151-742, South Korea*

[b] *Research Institute of Industrial Science and Technology, P.O. Box 135, Pohang 790-600, South Korea*

Received 21 November 2001; received in revised form 10 July 2002

Abstract

In the present paper, flow and heat transfer characteristics of confined impinging slot jets have been numerically investigated using a SIMPLE-based segregated streamline upwind Petrov–Galerkin finite element method. For laminar jets, it is shown that the skin friction coefficient approaches the grid-independent Galerkin solution and that the present simulation induces negligible false diffusion in the flow field. For turbulent jets, the k–ω turbulence model is adopted. The streamwise mean velocity and the heat transfer coefficient respectively agree very well with existing experimental data within limited ranges of parameters.

1. Introduction

Impinging jets are encountered in many industrial applications since they are effective tools to enhance and control localized heat or mass transfer. For instance, they are widely used for the cooling of turbine blades and electronic components as well as for the processing of materials such as paper, glass and fabric. Recently, laminar impinging jets are also being used for the cooling of micro-electronic devices. Therefore, there have been extensive experimental and numerical studies on impinging jets.

Gardon and Akfirat [1] measured local and average heat transfer coefficients for various Reynolds numbers and ratios of separation distance to nozzle width (H/B) for single and multiple impinging jet systems by using a flush-mounted heat-flow transducer. They showed that the maximum heat transfer coefficients at the stagnation point and the averaged Nusselt number over the target plate can be expressed as a simple function of the Reynolds number and H/B. By using heat flux method, van Heiningen [2] performed an experimental study of confined impinging slot jet system for various Reynolds numbers and $H/B = 2.6$ and 6. He showed that the second peak of the Nusselt number (Nu) can be larger than the first peak as the Reynolds number (Re) increases and that the first peak occurs away from the stagnation point. Furthermore, he obtained correlations of the heat transfer coefficients at the stagnation point, the second peak and the wall jet as functions of the Reynolds number and H/B. Ashforth-Frost et al. [3] obtained streamwise velocity profiles and turbulence quantities for $H/B = 4$ and 9.2 by using I-type hot-wire anemometry. They showed that the potential core of the confined jet is longer than that of the unconfined jet due to limited entrainment and spreading rate. They also pointed out that the second peak of Nu can be detected only when the target plate is placed within the potential core of the confined jet. Lin et al. [4] also performed an experimental study on heat transfer behaviors of a confined impinging slot jet for $190 < Re < 1537$ and $1 < H/B < 8$. They used T-type thermocouples for measuring the heat transfer coefficients on the target wall, and showed that the heat transfer characteristics are much more affected by Re than H/B.

* Corresponding author. Tel.: +82-2-880-7112; fax; +82-2-883-0179.

E-mail addresses: pthyun@shed.snu.ac.kr (T.H. Park), choi@vortex.snu.ac.kr (H.G. Choi), jyyoo@plaza.snu.ac.kr (J.Y. Yoo).

0017-9310/03/$ - see front matter
PII: S0017-9310(02)00270-3

Nomenclature

B	nozzle width
C_f	skin-friction coefficient, $\tau_w/(0.5\rho U_{in}^2)$
D	diameter of axisymmetric jet nozzle
H	distance between nozzle and target wall
h	heat transfer coefficient based on bulk temperature
I	turbulence intensity
K	thermal conductivity
k	turbulent kinetic energy
L	length of computational domain in the x-direction
Nu	Nusselt number, hB/K
P	pressure
Pr	Prandtl number, ν/κ
Pr_t	turbulent Prandtl number
Re	Reynolds number, $U_{in}B/\nu$
T	temperature
t	time
U_{in}	average jet velocity
u_i	velocity components
x, y	Cartesian coordinates
$\bar{y}$	height of the first element from the wall in the case of FEM, or the distance to the first grid point from the wall in the case of FVM

Greek symbols

α	closure coefficient (=0.556)
β	closure coefficient (=0.075)
β^*	closure coefficient (=0.09)
ε	dissipation rate of turbulent kinetic energy
κ	thermal diffusivity
ν	molecular kinematic viscosity
ν_t	turbulent kinematic viscosity, k/ω
ρ	fluid density
σ	closure coefficient ($=0.5$)
σ^*	closure coefficient ($=0.5$)
τ_{ij}	shear stress
τ_w	wall shear stress
ω	specific dissipation rate of turbulent kinetic energy

Subscripts

0	stagnation point
2	second peak point
cw	confining wall
in	inlet
tw	target wall

Superscripts

$+$	wall unit
$'$	turbulent fluctuation

As for computational studies, van Heiningen et al. [5] made a numerical prediction of a laminar semi-confined jet impinging on a permeable wall using finite difference method with hybrid or upwind scheme. The effect of nozzle exit velocity profile on the maximum friction coefficient was also considered, by noting that a flat velocity profile gives a smaller maximum friction coefficient than a parabolic velocity profile due to increased entrainment below the nozzle. Law and Masliyah [6] studied local mass transfer due to impingement of a confined laminar two-dimensional air jet on a flat surface both experimentally and numerically. They showed that the flow field can be divided into five different regions and that the streamwise variation of the local Sherwood number exhibits local extrema, which are attributed to the existence of flow recirculation region (see Fig. 9). Chen et al. [7] investigated high Schmidt number mass transfer to a line electrode in laminar slot-jet flows both experimentally and numerically, and showed that the maximum heat transfer coefficient occurs away from the stagnation point.

With the advancement in turbulence modeling and high performance computers [8,9], numerical simulations of turbulent impinging jets have been also carried out actively. The researchers are now able to perform large eddy simulation [10] or direct numerical simulation [11] of impinging jets. However, the arithmetic ability of the most up-to-date supercomputer has yet to be improved further in order to simulate impinging jets at practical Reynolds numbers. Thus, the use of turbulence modeling is still important for the simulation of impinging jets of practical interest. Craft et al. [9] examined the performance of one low Reynolds number k–ε model and three types of Reynolds stress models by applying them to the numerical prediction of open axisymmetric impinging jets. Behnia et al. [12] used the normal-velocity relaxation turbulence model proposed by Durbin [13] to predict an open axisymmetric impinging jet. Some of the recent numerical studies of turbulent impinging jets have used the k–ω model proposed by Wilcox [14] since the basic assumption on which the k–ε model is established is not valid in the stagnation region. Heyerichs and Pollard [15] assessed the performance of the k–ω model and several versions of the k–ε model by considering both separating and impinging turbulent flows with heat transfer. Their results indicated that the k–ω model is superior to the standard k–ε model for prediction of complex turbulent flows and is numerically easy to implement. Recently, Chen and Modi [16] studied mass transfer in turbulent impinging slot jets

using the k–ω model and compared the velocity fields with those obtained experimentally by Ashforth-Frost et al. [3]. Besides, their numerical heat transfer data showed a fair agreement with the experimental data of Gardon and Akfirat [1], with a secondary peak in Nu appearing in both of them.

It is now noted that although there have been many numerical studies on laminar and turbulent confined or unconfined impinging jets, there have been very few numerical researches [17] on how a spatial discretization method affects the solution. The structure of an impinging jet is so complex that its numerical prediction could be severely affected by false diffusion (artificial diffusion) of an upwind type numerical method. Therefore, we are to introduce streamline upwind Petrov–Galerkin (SUPG) method [18], which is widely adopted in conjunction with finite element method due to its robustness and reduced numerical diffusion. In order to verify the effectiveness of SUPG method for impinging jets, we first obtain a grid-independent solution of a laminar impinging jet for a certain Reynolds number and compare it with the solutions obtained by SUPG and other upwind schemes. For turbulent flow calculation, the k–ω model is adopted in the present study because it is known to be quite effective in the recirculating regions by previous researchers [15,16]. To discretize the Navier–Stokes equations, semi-implicit method for pressure-linked equations (SIMPLE) with equal-order finite element method proposed by Rice and Schnipke [19] is used, because it was shown by Choi and Yoo [20] that SIMPLE algorithm combined with equal-order FEM incorporating SUPG method performs robustly and prevents the solution of a high Reynolds number flow problem from being spoiled significantly by false diffusion.

In Section 2, the governing equations and numerical method are described. In Section 3, numerical results for laminar and turbulent impinging jets are given and turbulent heat transfer characteristics of a confined impinging jet are sought through the estimation of Nu along the target wall. Conclusions are drawn in Section 4.

2. Numerical methods

2.1. Governing equations

Governing equations are the following two-dimensional incompressible Navier–Stokes, continuity and energy equations:

Continuity,

$$\frac{\partial u_i}{\partial x_i} = 0 \tag{1}$$

Momentum,

$$\frac{\mathrm{D}u_i}{\mathrm{D}t} = -\frac{1}{\rho}\frac{\partial P}{\partial x_i} + \frac{\partial}{\partial x_j}\left((\nu + \nu_\mathrm{t})\,\mathrm{D}_{ij}\right) \tag{2a}$$

$$\mathrm{D}_{ij} = \frac{\partial u_i}{\partial x_j} + \frac{\partial u_j}{\partial x_i} \tag{2b}$$

Energy,

$$\frac{\mathrm{D}T}{\mathrm{D}t} = \frac{\partial}{\partial x_i}\left[\left(\frac{\nu}{Pr} + \frac{\nu_\mathrm{t}}{Pr_\mathrm{t}}\right)\frac{\partial T}{\partial x_i}\right] \tag{3}$$

where the Prandtl number and turbulent Prandtl number for air are given as follows:

$$\begin{aligned} Pr &= 0.72 \\ Pr_\mathrm{t} &= 0.9 \end{aligned} \tag{4}$$

According to Kays and Crawford [21], the molecular Prandtl number has very little effect on the turbulent Prandtl number which is close to unity in most of fluid flows, except in a region close to wall ($y^+ < 6$), where Pr_t varies with y^+. However, a constant turbulent Prandtl number is used in the present study since, according to Behnia et al. [12], there is indistinguishable difference between the result obtained with some widely used constant Pr_t and that with the Kays-and-Crawford formula [21] (see also Fig. 8 of Chen and Modi [16]). For turbulence modeling, k–ω model proposed by Wilcox [14] is implemented.

$$\frac{\mathrm{D}k}{\mathrm{D}t} = \frac{\tau_{ij}}{\rho}\frac{\partial u_i}{\partial x_j} - \beta^* k\omega + \frac{\partial}{\partial x_j}\left[(\nu + \sigma^*\nu_\mathrm{t})\frac{\partial k}{\partial x_j}\right] \tag{5a}$$

$$\frac{\mathrm{D}\omega}{\mathrm{D}t} = \alpha\frac{\omega}{k}\frac{\tau_{ij}}{\rho}\frac{\partial u_i}{\partial x_j} - \beta\omega^2 + \frac{\partial}{\partial x_j}\left[(\nu + \sigma\nu_\mathrm{t})\frac{\partial \omega}{\partial x_j}\right] \tag{5b}$$

where k is the turbulent kinetic energy, ω is the specific dissipation rate of the turbulent kinetic energy. They are related to ν_t by

$$\nu_\mathrm{t} = \frac{k}{\omega} \tag{6}$$

The closure coefficients are

$$\begin{aligned} &\alpha = 0.556, \quad \beta = 0.075, \quad \beta^* = 0.09, \\ &\sigma = 0.5, \quad \sigma^* = 0.5 \end{aligned} \tag{7}$$

SIMPLE-based SUPG finite element method developed by Choi and Yoo [20] is used for solving the transport equations of momentum, energy, turbulent kinetic energy and energy dissipation rate. For more detailed exemplification of the SUPG formulation of those transport equations and the derivation of the pressure equations, reference should be made to Choi and Yoo [20].

Then the overall iterative procedure can be explained as follows. The momentum equation is solved with a guessed pressure field to obtain a velocity field, which

does not necessarily satisfy the continuity equation. The velocity field is then corrected by the pressure field which is constructed by solving the Poisson type pressure equation so that the divergence-free constraint can be satisfied. The same procedure is repeated until the required convergences of both the momentum and continuity equations are achieved. For turbulent flows, k–ω model equations are solved at every iteration after both the momentum and continuity equations are solved. Once the converged turbulent flow field is obtained, energy equation is solved. In the present study, it is assumed that the fluid density and viscosity are independent of temperature variation. Therefore, the energy equation is decoupled from the momentum equation.

2.2. Boundary conditions

The computational domain is shown in Fig. 1, where, using the symmetry of the present problem, only half of the flow domain is considered. The length of the computational domain in the x-direction is approximately $L = 100$ B, which is quite longer than that of other existing computations [16], to ensure the traction-free boundary condition at the exit. From numerical experiment, we have noticed that the region of adverse pressure gradient (recirculation zone) is so large that the computational domain must be extended long enough to attain a fully developed velocity profile at the exit. At walls, no-slip conditions are used for the velocity components, constant temperature conditions are used such that $T_{\mathrm{tw}} = 310$ K and $T_{\mathrm{cw}} = 300$ K, and the following conditions proposed by Wilcox [14] are used for k and ω:

$$\omega = \frac{6\nu}{0.075\bar{y}^2}, \quad k = 0,$$

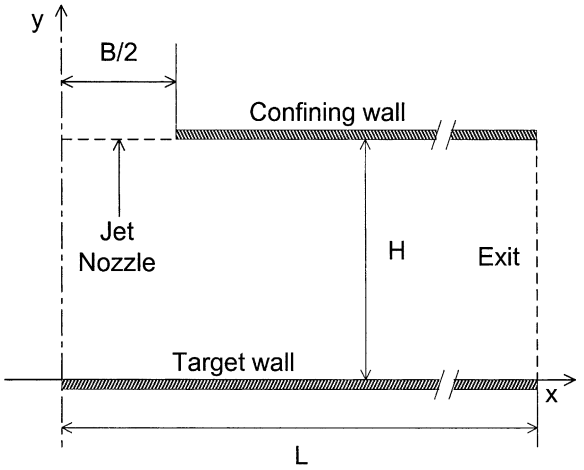

Fig. 1. Schematic diagram of the flow domain considered in the present study.

where $\bar{y}$ is the height of the first element from the wall. It is also noted that y^+ should be less than about 2.5 (see [14] for more details). Along the symmetry line, the following conditions are used:

$$u = 0, \quad \frac{\partial v}{\partial x} = 0, \quad \frac{\partial k}{\partial x} = 0, \quad \frac{\partial \omega}{\partial x} = 0, \quad \frac{\partial T}{\partial x} = 0$$

At the inlet, fully developed parabolic velocity profile is used in the case of laminar impinging jet and uniform velocity profile in the case of turbulent jet. Also, Dirichlet boundary conditions are used for k, ω, T, and ν_{t} at the inlet:

$$k_{\mathrm{in}} = \frac{3}{2}(IU_{\mathrm{in}}^2)^2, \quad \omega_{\mathrm{in}} = \frac{k}{\nu_{\mathrm{t}}}, \quad T_{\mathrm{in}} = 300 \text{ K}, \quad \nu_{\mathrm{t}} = 0.01\nu,$$

where U_{in} is the velocity at the inlet and I is the turbulent intensity defined as follows:

$$I = \sqrt{((u'^2 + v'^2 + w'^2)/3/U_{\mathrm{in}}^2}$$

The uniform distributions of k and ω at the inlet are incompatible with the boundary conditions of k and ω at the confining wall since k goes to zero smoothly toward the wall and ω is proportional to $1/y^2$ near the wall. However, since the point shared by the inlet and the confining wall is a kind of singular point (the confining wall is perpendicular to the inlet flow), uniform distributions of k and ω are used for convenience' sake as was done in many previous simulations [14–16].

At the exit, Neumann boundary conditions are used for all flow variables, u, v, k, ω and T. As mentioned in Section 2.1, the mass conservation is satisfied by solving the following elliptic type pressure equation, which is derived by imposing the divergence-free constraint.

$$\int_{\Omega_e} \left[\frac{\partial w_i}{\partial x}\left(N_j K_j \frac{\partial N_k}{\partial x} p_k\right) + \frac{\partial w_i}{\partial y}\left(N_j K_j \frac{\partial N_k}{\partial y} p_k\right) \right] \mathrm{d}A_e = \int_{\Omega_e} \left(\frac{\partial w_i}{\partial x} N_j \hat{u}_j + \frac{\partial w_i}{\partial y} N_j \hat{v}_j \right) \mathrm{d}A_e - \int_{\Gamma_e} (w_i \hat{\boldsymbol{u}} \cdot \bar{\boldsymbol{n}}) \, \mathrm{d}S_e, \tag{8}$$

where the hat velocities, $\hat{u}_j$, $\hat{v}_j$ are obtained from the discretized momentum equation (for more details including the nomenclature, see Refs. [19,20]). The boundary condition is imposed by adding a sort of mass flux along the boundary of the computational domain (second term on the right hand side of Eq. (8)). Since mass fluxes are zero at the symmetry line, the target wall and the confining wall, they need to be prescribed only at the inlet and exit. Those mass fluxes act as a source term in the pressure Eq. (8).

2.3. Convergence criterion

The maximum error $e_{\max}$ has been defined as

$$e_{\max} = \max_{i=1,N_{\mathrm{t}}} |\phi_i^n - \phi_i^{n-1}| \langle 10^{-5},$$

where N_t denotes the total number of nodes, the subscript i denotes the specific node point, the superscript n denotes the iteration level and ϕ denotes the flow variables u, v, p. The equation for each variable was solved iteratively until the above convergence criterion is achieved.

2.4. Grid arrangement

In order to resolve the steep gradient of the flow variable near the wall, this non-uniform grid clustered at both walls is used. The following equation [22] is used to obtain this clustered grid in the y-direction:

$$y = H\frac{(2\alpha+\beta)[(\beta+1)/(\beta-1)]^{(\eta-\alpha)/(1-\alpha)}+2\alpha-\beta}{(2\alpha+1)\{1+[(\beta+1)/(\beta-1)]^{(\eta-\alpha)/(1-\alpha)}\}} \quad (9)$$

where $\alpha = 1/2$, $\eta = 1/N$ (N is the number of grid points in the y-direction), and $\beta > 1.0$ is a clustering factor. As β approaches 1.0, a more clustered grid is obtained. In the x-direction, a uniform grid is used at the inlet region and a clustered grid toward the inlet is used along the wall using Eq. (9) and $\alpha = 0$.

3. Numerical results

First of all, a laminar impinging jet at a moderate Reynolds number is solved with Galerkin method (which is equivalent to central difference scheme of FDM) to be compared with the solutions obtained by adopting SUPG method and with other existing results. Since there have been no available experimental studies which can be used for quantitative comparison with the present study, we are mainly concerned with the numerical accuracy of the present simulation. In other words, the laminar impinging jet calculation can be regarded as a part of code validation procedure for the turbulent impinging jet calculation, where comparisons with extant experimental data are to be made.

3.1. Laminar impinging jet

In the present study, all Galerkin solutions of laminar impinging jet are grid-independent solutions which we use to rigorously estimate the amount of false diffusion of solutions obtained by using upwind type schemes. In Fig. 2, various upwind solutions including SUPG have been compared with the Galerkin grid-independent solution for $Re = 220$ and $H/B = 2$. With FLUENT™, both first-order upwind and QUICK schemes with the identical 100×80 non-uniform grid as used in the SUPG simulation have been adopted. The result of Chen et al. [7], who used cell-centered FVM based on artificial compressibility method, and that obtained by first-order upwind scheme of FLUENT™ do not reveal any secondary vortex, which is considered to be due to artificial numerical diffusion. Although the solution obtained by QUICK scheme of FLUENT™ shows the secondary vortex clearly, the streamline pattern near the stagnation region is a little different from that of the grid-independent Galerkin solution, which results in the wrong estimation of friction coefficient near the stagnation region to be shown later in Fig. 3. On the other hand, it can be noted that the present SUPG solution shows the existence of the secondary vortex clearly, which is comparable to that of the Galerkin solution. It is reminded that SUPG method is precisely reduced to the Galerkin method only when the Peclet number of every element is negligibly small. Therefore, there is always some numerical diffusion with SUPG method unless a very fine grid is used [23]. However, it is noteworthy that the solution of SUPG formulation is quite comparable to that of the Galerkin formulation when a reasonable number of grid points is used. The accuracy of SUPG formulation for high Reynolds number flows, as is well known, comes from the fact that upwinding is applied not along the grid line direction but along the flow direction [18].

Fig. 3 compares the distributions of the skin friction along the target wall obtained from various upwind methods with that from the grid-independent Galerkin solution. Peak of the C_f curve appears near the stagnation region because the axial flow in the y-direction is deflected and turned into the streamwise flow in the x-direction so that the axial flow decelerates with the acceleration of the streamwise flow. The occurrence of negative values of C_f represents the existence of a recirculation zone.

As shown here, upwind schemes of finite volume method cannot predict well the skin-friction coefficient near the stagnation region as well as the recirculation region. Note that the C_f curve drawn from SUPG solution follows that from the Galerkin solution quite well. It is conjectured that upwind schemes of finite volume method, in which upwinding is applied along the grid line direction, are not suitable for impinging jet calculation since the flow direction changes abruptly in the stagnation region.

3.2. Turbulent impinging jet

As a further code validation for turbulent flow calculation, which uses an equal-order FEM based on SIMPLE algorithm and the k–ω model, a developing turbulent channel flow has been solved for $Re = 5700$, where the Reynolds number is based on half-height of the channel and centerline velocity. Fig. 4 shows that the velocity profile obtained in the present study agrees well with the LDV data [24] for turbulent channel flow.

With this background, numerical simulation of the turbulent confined impinging jet for $Re = 20,000$ and

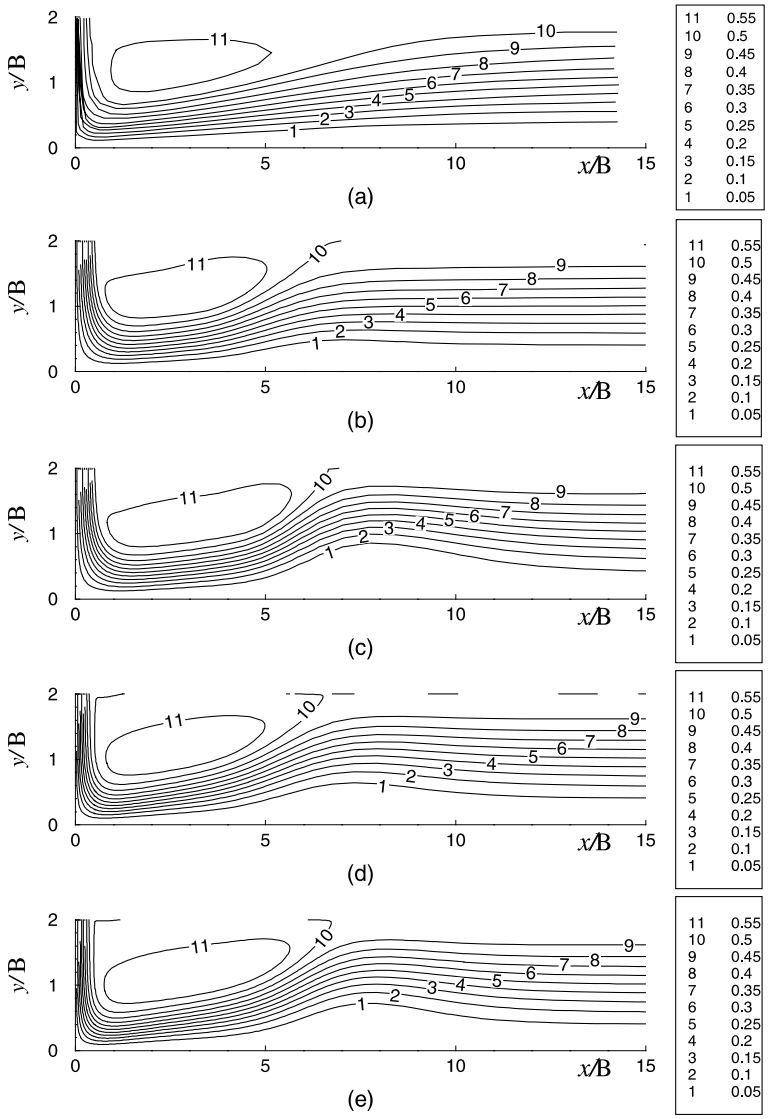

Fig. 2. Comparison of streamlines for $Re = 220$ and $H/B = 2$: (a) [7] (80×80 grid); (b) first-order upwind scheme of FLUENT™ (100×80 grid); (c) third-order upwind (QUICK) scheme of FLUENT™ (100×80 grid); (d) present simulation with SUPG method (100×80 grid); (e) Galerkin grid-independent solution (150×130 grid).

$H/B = 4$ has been performed and the results are compared with the experimental data of Ashforth-Frost et al. [3]. A 350×100 non-uniform grid with clustered grid lines near the walls is used.

At the inlet, uniform velocity profile is given and the experimental value of turbulence intensity (1%) is imposed. Fig. 5 shows the distributions of the x-component of the mean velocity at various downstream locations of the wall jet, which are compared with previous experimental [3] and numerical [16] results. It is noted that, to account for the effect of false diffusion on the numerical solutions, the present study uses the same k–ω turbulence model and an equivalent grid resolution of 350×100, used by Chen and Modi [16]. In Fig. 5(a), it is shown that, at $x/B = 1$ and 2, the present calculation is in excellent agreement with the experimental result obtained by Ashforth-Frost et al. [3], while there is some discrepancy between the present study and Chen and Modi [16]. Considering that in this region the axial flow is deflected and turned into an accelerating flow in the x-direction, flow measurements using constant-temperature hot-wire anemometry with a boundary-layer probe is believed to be most accurate. Therefore, it can be argued that the present calculation with reduced false

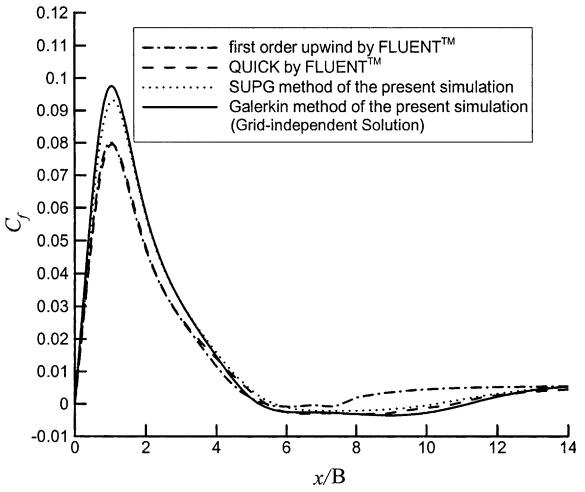

Fig. 3. Comparison of skin-friction coefficient distributions obtained by SUPG method, Galerkin method and upwind methods using FLUENT™ for $Re = 220$ and $H/B = 2$.

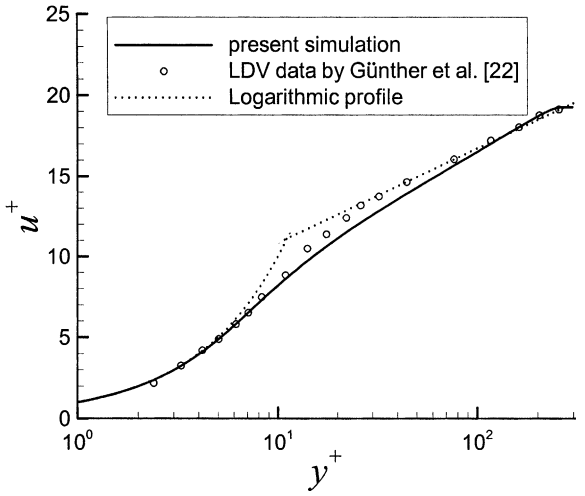

Fig. 4. Comparison of velocity profile with previous experimental data in channel flow.

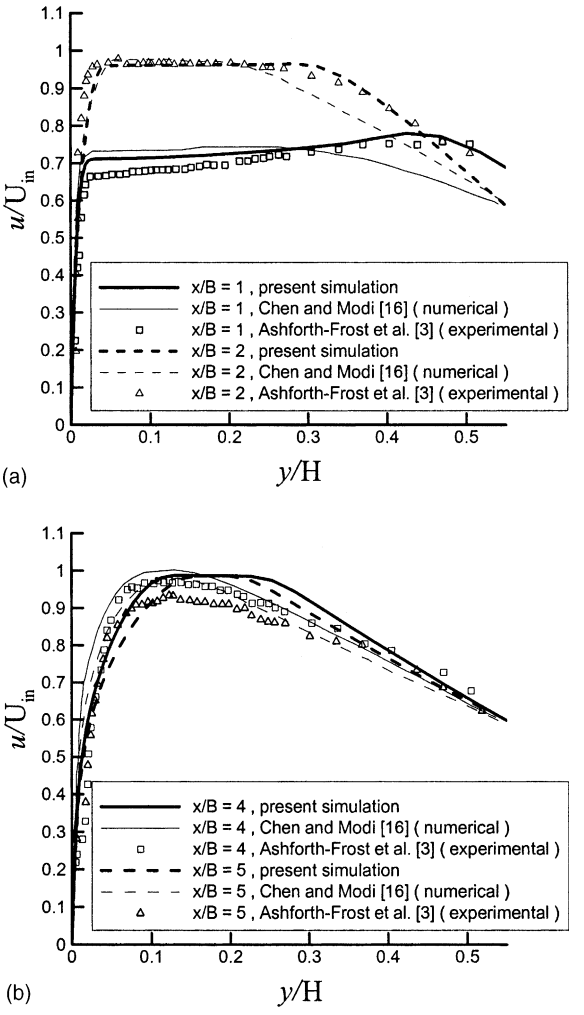

Fig. 5. Comparison of computed x-component of the mean velocity with the experimental data for $Re = 20{,}000$ and $H/B = 4$: (a) $x/B = 1$, 2; (b) $x/B = 4$, 5.

diffusion is in better agreement with the experimental data than Chen and Modi's [16] calculation because the latter might have been affected by false diffusion. However, Fig. 5(b) shows that further downstream the present velocity profiles agree only qualitatively with the experimental results of Ashforth-Frost et al. [3]. For instance, at $x/B = 4$, maximum values of both profiles appear as plateaus, not as peak points on smooth curves, in the respective ranges of $0.05 < y/H < 0.2$ for Ashforth-Frost et al. [3] and $0.1 < y/H < 0.25$ for the present study. At $x/B = 5$, plateaus are seemingly narrowed down to peak points. This trend is not observed in the calculation of Chen and Modi [16] although their results seem to be a little closer to the experiment quantitatively. In this region it is considered that deceleration of the bulk velocity near the wall occurs as the jet spreads wider downstream [3], which causes the growth of the secondary vortex. This may possibly explain the quantitative difference between the two studies, and calls for further investigations on the flow structure downstream of the stagnation region. It is noted in passing that the calculation of Chen and Modi [16] exhibits a different trend from the other two studies.

The Nu distribution along the target wall has been obtained for $Re = 11{,}000$ and $H/B = 2.6$, and compared with existing experimental data of van Heiningen [2] for $Re = 10{,}200$ and $H/B = 2.6$, and numerical data of Heyerichs and Pollard [15] for $Re = 11{,}000$ and

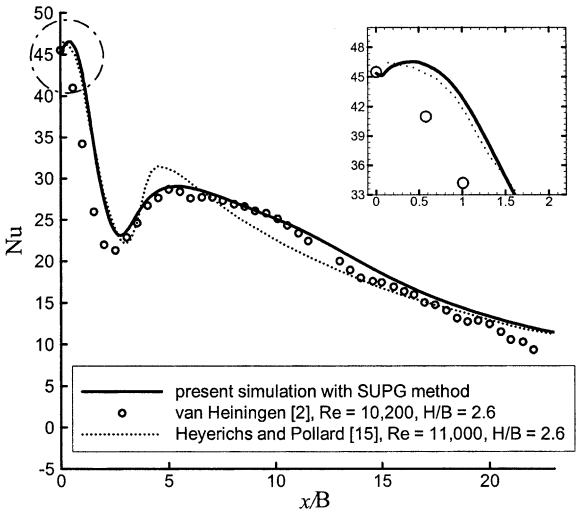

Fig. 6. Comparison of the Nusselt number curve with experimental data and other simulation result for $Re = 11{,}000$ and $H/B = 2.6$.

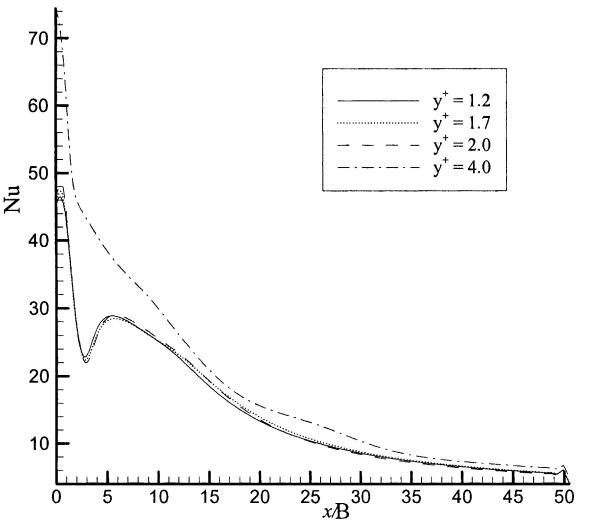

Fig. 7. Nusselt number curves for various values of y^+ and $H/B = 2.6$.

$H/B = 2.6$, as shown in Fig. 6. At the inlet, the experimental value of the turbulence intensity (4%) is given and y^+ at the nearest node from the wall is kept to be around 1.0. Overall, the results of the present study and Heyerichs and Pollard [15] using the k–ω model give accurate estimations of *Nu*. However, compared to the numerical result of Heyerichs and Pollard [15], the present result predicts the second peak of *Nu* more accurately and the slope of the curve after the second peak of *Nu* is milder than theirs, following the experimental result more precisely. It is understood that those differences from the two numerical simulations come from the fact that the present numerical simulation predicts a flow field with strong adverse pressure gradient more accurately than Heyerichs and Pollard [15]. As can be noticed, the major difference between the two simulations occurs for $2.5 < x/B < 15.0$, where a strong adverse pressure gradient exists. The fact that the present simulation needs a longer computational domain than others [16] is a strong implication of the fact that the present numerical scheme is less susceptible to numerical diffusion. It should be again noted that the effect of numerical diffusion is strong near a recirculation region where the flow direction is not aligned with the grid line [25]. Another interesting phenomenon of turbulent impinging jet heat transfer is that the first peak of *Nu* occurs not at the center of the target wall but at $x/\mathrm{B} \sim 0.5$, as shown in the inset of Fig. 6. This was observed from the experiment of both van Heiningen [2] and Chen et al. [7], and is confirmed numerically in the present study.

Fig. 7 shows the effect of the distance to the first node point from the wall on the distribution of the Nusselt number along the wall. It is confirmed that when using the k–ω model, the condition that y^+ should be less than about 2.5 has to be satisfied. That is, the solutions from different values of y^+ are almost coincident only if this condition is satisfied. Fig. 8 shows the effect of *Re* on *Nu* for $H/B = 2.6$, compared with the experiment of van Heiningen [2]. The Nusselt numbers of the present simulation at the stagnation are in good agreement with the experimental data, but the magnitude and position of the second peaks of the present simulation disagree more with the experimental data as *Re* increases. Presently we are not certain whether the difference between

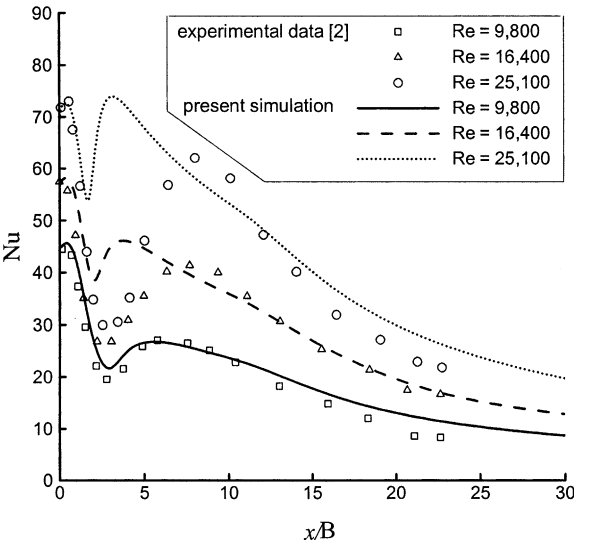

Fig. 8. Effect of Reynolds number on the Nusselt number curve with the experimental data [2] for $H/B = 2.6$.

the experiment and the present simulation comes mainly from three-dimensionality or some other origin. However, according to the results of Phares et al. [26] and Meola et al. [27], the impinging jet flow shows a strong three-dimensionality near the transition after the stagnation (laminar) region and the transition occurs near the minimum of the Nusselt number. From Fig. 8, it seems that the transition occurs at $x/B \sim 2$ in the present case. Therefore, it is conjectured that the difference may come from the deficiency of the present two-dimensional k–ω code, which is unable to model the transition and the corresponding three-dimensionality. Such a trend can also be found in other previous studies [28]. In fact, numerical simulations of both the present study and Chalupa et al. [28] reveal that as the Reynolds number increases the second peak of the Nu distribution approaches the position of the first peak and its magnitude increases at a faster rate than the experimental data [2]. Fig. 9 shows that beyond a certain threshold value of Re, the second peak of the present numerical calculation is larger than the first peak. This trend is in qualitative agreement with the experiment of van Heiningen [2], where the value of the second peak is larger than the first peak at the Reynolds number beyond 47,900. At this point, it is conjectured that, as the Reynolds number increases, the three-dimensional effect comes into play so that our two-dimensional calculation may not reflect the physical flow situation precisely. A further discussion on this aspect will be given at the last part of this section.

Fig. 10 shows the distributions of Nu and the pressure coefficient along the target wall for various values of H/B and $Re = 11{,}000$, where the same inlet turbulence intensity and grid system as in Fig. 6 are used. The

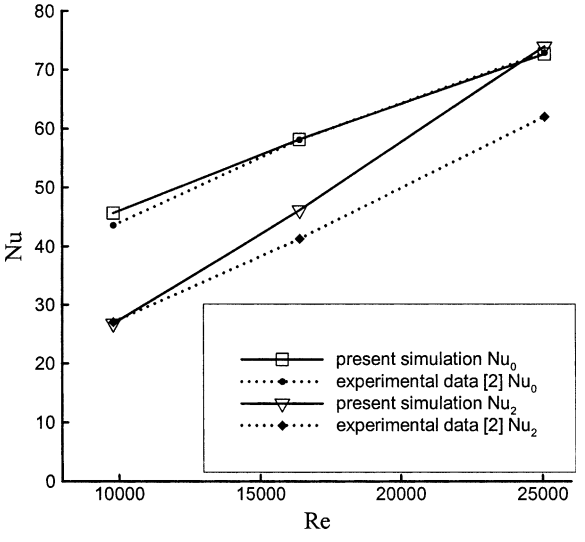

Fig. 9. Comparison of Nu_0 and Nu_2 with experimental data [2] for $H/B = 2.6$.

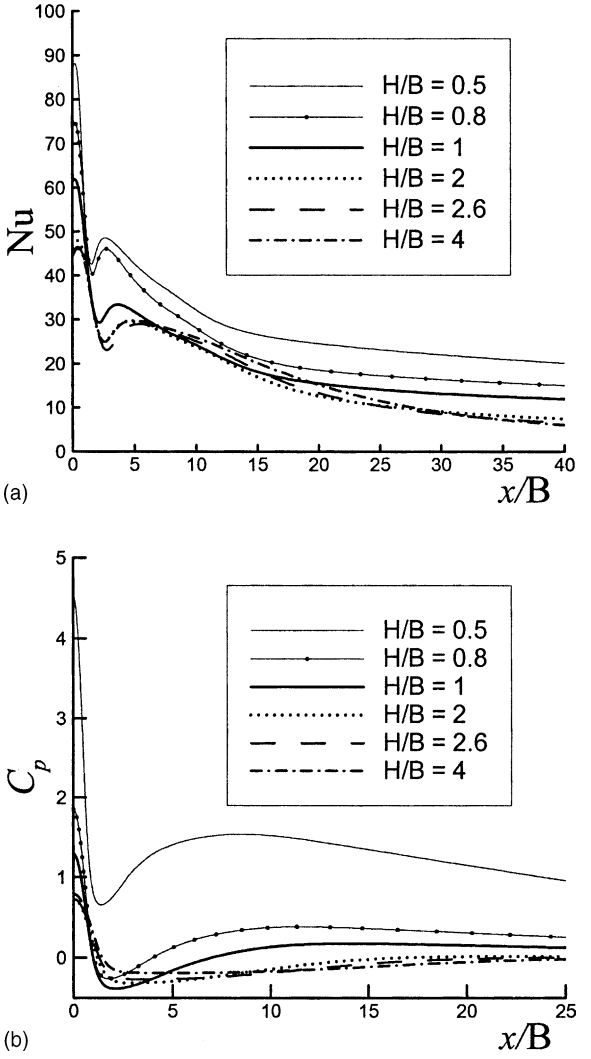

Fig. 10. Distributions of (a) Nu and (b) the pressure coefficient for various values of H/B and $Re = 11{,}000$.

position of local minimum of Nu moves toward the center of the target wall as H/B decreases. This is clearly related to the decrease of the primary vortex size as H/B decreases, as shown in Fig. 11. It is also noted that the slope of the Nu curve after the second peak becomes steeper as H/B decreases, because the region of adverse pressure gradient becomes smaller as H/B decreases.

Fig. 12 shows a comparison of the maximum Nu as a function of H/B for a given Reynolds number. Cadek [29] performed an experimental study of confined impinging slot jet for various values of H/B and the Reynolds number, and pointed out that the value of the first peak of the Nu curve increases as H/B increases for $1 < H/B < 8$. The experimental study by Gardon and Akfirat [1] also reveals a similar behavior. According to

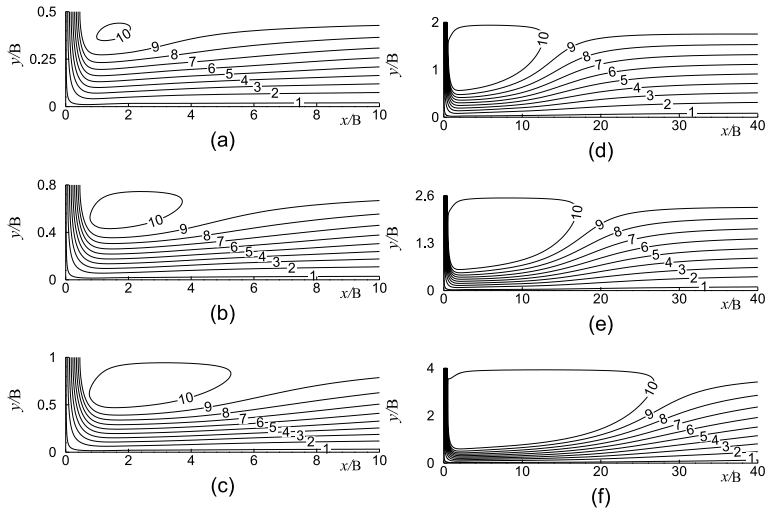

Fig. 11. Comparison of streamlines for various values of H/B and $Re = 11{,}000$: (a) 0.5, (b) 0.8, (c) 1.0, (d) 2.0, (e) 2.6, (f) 4.0 (the values of the streamfunction are 0, 0.055, 0.11, 0.165, 0.22, 0.275, 0.33, 0.385, 0.44, 0.495, 0.55, which are symbolized by the numbers 1, 2, 3, 4, 5, 6, 7, 8, 9, 10, 11, respectively).

these previous studies, this phenomenon is attributed to the increase of turbulent intensity in the stagnation region as H/B increases up to approximately 8, although the maximum centerline velocity decreases as H increases beyond the potential core length. However, this phenomenon is not reproduced by the present simulation. In fact, Chen and Modi [16] did not reveal this phenomenon either in their two-dimensional calculation of mass transfer in turbulent impinging slot jets. Maximum spatially averaged Sherwood numbers in the impingement region are nearly independent of H/B, which is quite similar to the present two-dimensional calculation (see Fig. 11 of Ref. [16]). As a consequence, it is conjectured that the difference between the two-dimensional simulation and the experiment regarding the variation of the maximum Nu comes from the three-dimensionality of the turbulent flow. On the other hand, it has been found that the maximum value of Nu increases as H/B decreases for $H/B < 1$. The same phenomenon was reported by Lytle and Webb [30] who performed an experimental study of circular air jet impingement heat transfer for low nozzle-plate spacings using an infrared thermal imaging technique. They proposed that the distribution of the peak Nu can be derived theoretically with the following power-law:

$$\frac{Nu_0}{Re^{1/2}} = 0.821(H/D)^{-0.288} \tag{10}$$

Their experimental data are in good agreement with this equation, especially for low nozzle-plate spacings ($H < 1.0$). From the present simulation, it has been found that the maximum Nu abruptly increases when H/B becomes smaller than approximately 1.0, showing a similar trend to the theoretical correlation (10) and also the experimental data of Lytle and Webb [30]. It should be noted that equation (10) derived for a circular air jet impingement is appropriate to a low nozzle-plate spacing. Therefore, it can be thought that the difference of the maximum heat transfer characteristics between a slot jet and a circular jet becomes less as nozzle-plate spacing decreases.

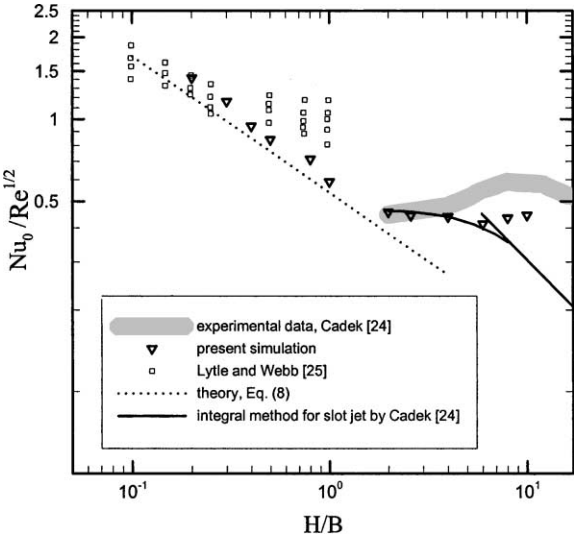

Fig. 12. Comparison of the maximum Nusselt number for various values of H/B and $Re = 11{,}000$.

4. Conclusions

A SIMPLE-based finite element code using streamline upwind Petrov–Galerkin method and adopting k–ω

model proposed by Wilcox [14] has been developed to predict the flow and heat transfer characteristics of two-dimensional confined impinging slot jets.

In order to assess the effect of false numerical diffusion on a laminar confined impinging slot jet, a Galerkin grid-independent solution is obtained and compared with the present SUPG solution, existing numerical solutions in the literature, and the solutions obtained by using commercial code FLUENT™. It has been shown that SUPG formulation greatly reduces the false diffusion compared to the finite volume formulation, in the prediction of the complex flow field involving the stagnation region.

For turbulent impinging jets, the x-component of the mean velocity is shown to be in excellent agreement with the experimental data where the wall jet is developing. Then, the calculated Nu distribution is also shown to be in good agreement with the experimental data for low Reynolds number range. However, as the Reynolds number increases, the magnitude and position of the second peak of the Nu plot disagree more with the experimental data, which is common to all two-dimensional numerical simulations. Lastly, for $H/B < 1$, the maximum Nu increases as H/B decreases, which qualitatively agrees well with the theoretical power–law relationship obtained for circular air jet impingement heat transfer.

Thus, an extension of the present SUPG finite element method to three-dimensional or at least axisymmetric flow problems may constitute a very interesting future study.

Acknowledgements

This work has been supported by Research Institute of Industrial Science and Technology and partially supported by the BK21 Project, Ministry of Education and Human Resources Development, Republic of Korea. The authors are grateful to Professor A.R.P. van Heiningen for providing a copy of his Ph.D. thesis and for his valuable comments on this work.

References

[1] R. Gardon, J.C. Akfirat, Heat transfer characteristics of impinging two dimensional air jets, Transactions of the ASME, J. Heat Transfer 88 (1966) 101–108.

[2] A.R.P. van Heiningen, Heat transfer under an impinging slot jet, Ph.D. thesis, McGill University, Montreal, 1982.

[3] S. Ashforth-Frost, K. Jambunathan, C.F. Whitney, Velocity and turbulence characteristics of a semiconfined orthogonally impinging slot jet, Experim. Thermal Fluid Sci. 14 (1997) 60–67.

[4] Z.H. Lin, Y.J. Chou, Y.H. Hung, Heat transfer behaviors of a confined slot jet impingement, Int. J. Heat Mass Transfer 40 (5) (1997) 1095–1107.

[5] A.R.P. van Heiningen, A.S. Mujumdar, W.J.M. Douglas, Numerical prediction of the flow field and impinging heat transfer caused by a laminar slot jet, Transactions of the ASME, J. Heat Transfer 98 (1976) 654–658.

[6] H.-S. Law, J.H. Masliyah, Mass transfer due to a confined laminar impinging two-dimensional jet, Int. J. Heat Mass Transfer 27 (4) (1984) 529–539.

[7] M. Chen, R. Chalupa, A.C. West, V. Modi, High Schmidt mass transfer in a laminar impinging slot jet flow, Int. J. Heat Mass Transfer 43 (21) (2000) 3907–3915.

[8] D. Cooper, D.C. Jackson, B.E. Launder, G.X. Liao, Impinging jet studies for turbulence model assessment—I. Flow field experiments, Int. J. Heat Mass Transfer 36 (10) (1993) 2675–2684.

[9] T.J. Craft, L.J.W. Graham, B.E. Launder, Impinging jet studies for turbulence model assessment—II. An examination of the performance of four turbulence models, Int. J. Heat Mass Transfer 36 (10) (1993) 2685–2697.

[10] M. Olsson, L. Fuchs, Large eddy simulations of a forced semiconfined circular impinging jet, Phys. Fluids 10 (2) (1998) 476–486.

[11] S. Satake, T. Kunigi, Direct numerical simulation of an impinging jet into parallel disks, Int. J. Numer. Meth. Heat Fluid Flow 8 (7) (1998) 768–780.

[12] M. Behnia, S. Parneix, P.A. Durbin, Prediction of heat transfer in an axisymmetric turbulent jet impinging on a flat plate, Int. J. Heat Mass Transfer 41 (12) (1998) 1845–1855.

[13] P. Durbin, Separated flow computations with the k–ε–v^2 model, AIAA J. 33 (4) (1995) 659–664.

[14] D.C. Wilcox, in: Turbulence Modeling for CFD, DCW Industries, Inc, La Cañada, CA, 1994, pp. 84–87.

[15] K. Heyerichs, A. Pollard, Heat transfer in separated and impinging turbulent flows, Int. J. Heat Mass Transfer 39 (12) (1996) 2385–2400.

[16] Q. Chen, V. Modi, Mass transfer in turbulent impinging slot jet, Int. J. Heat Mass Transfer 42 (5) (1999) 873–887.

[17] P.Y. Tzeng, C.Y. Soong, C.D. Hsieh, Numerical investigation of heat transfer under confined impinging turbulent slot jet, Numer. Heat Transfer Part A 35 (1999) 903–924.

[18] A.N. Brooks, T.J.R. Hughes, Streamline upwind/Petrov–Galerkin formulations for convection dominated flows with particular emphasis on the incompressible Navier–Stokes equations, Comput. Meth. Appl. Mech. Eng. 32 (1982) 199–259.

[19] J.G. Rice, R.T. Schnipke, An equal order velocity pressure formulation that does not exhibit spurious pressure modes, Comput. Meth. Appl. Mech. Eng. 58 (1986) 135–149.

[20] H.G. Choi, J.Y. Yoo, Streamline upwind scheme for the segregated formulation of the Navier–Stokes equation, Numer. Heat Transfer Part B 25 (1994) 145–161.

[21] W.M. Kays, M.E. Crawford, Convective Heat and Mass Transfer, third ed., McGraw-Hill, New York, 1993.

[22] K.A. Hoffmann, S.T. Chiang, Computational Fluid Dynamics for Engineers, vol. I, Engineering Education System™, 1993.

[23] J.Y. Sung, H.G. Choi, J.Y. Yoo, Time-accurate computation of unsteady free surface flows using an ALE segregated equal-order FEM, Comput. Meth. Appl. Mech. Eng. 190 (2000) 1425–1440.
[24] A. Günther, D.V. Papavassiliou, M.D. Warholic, T.J. Hanratty, Turbulent flow in a channel at a low Reynolds number, Experim. Fluids 25 (1998) 503–511.
[25] S.V. Patankar, Numerical Heat Transfer, McGraw-Hill, New York, 1980.
[26] D.J. Phares, G.T. Smedley, R.C. Flagan, The wall shear stress produced by the normal impingement of a jet on a flat surface, J. Fluid Mech. 418 (2000) 351–375.
[27] C. Meola, L. de Luca, G.M. Carlomagno, Azimuthal instability in an impinging jet: adiabatic wall temperature distribution, Experim. Fluids 18 (1995) 310–503.
[28] R. Chalupa, M. Chen, V. Modi, A.C. West, High Schmidt mass transfer in a turbulent impinging slot-jet flow, Int. J. Heat Mass Transfer 44 (2001) 3775–3785.
[29] F. F. Cadek, A fundamental investigation of jet impingement heat transfer, Ph.D. thesis, University of Cincinnati, Cincinnati, OH, 1968.
[30] D. Lytle, B.W. Webb, Air jet impingement heat transfer at low nozzle-plate spacings, Int. J. Heat Mass Transfer 37 (1994) 1687–1697.